Nanoscale Dolmen Structure Exhibiting A Tunable Fano Resonance

by

NICHOLAS F. BEIER

Advisor:

DR. RICHARD F. HAGLUND, JR.

Submitted to the DEPARTMENT OF PHYSICS AND ASTRONOMY at VANDERBILT UNIVERSITY in partial fulfillment of the requirements for an HONORS DEGREE IN PHYSICS

to be awarded on

May 13, 2016

VANDERBILT UNIVERSITY

ABSTRACT

A Fano resonance is an asymmetric, resonant scattering phenomenon which occurs in a multitude of fields, such as atomic physics, nuclear physics, nonlinear optics, and nanophotonics. The Fano resonance is a many-particle excitation arising from a single-particle excitation, and occurs due to the interference of a narrow discrete resonance overlapping with a spectrally broad resonance. Multi-element nanoparticles are explored as a means to realize this resonance type, which has a characteristic, steep dispersion useful in sensors, among other devices. A gold dolmen nanostructure consisting of a bright, radiative, dipolar mode coupled with a dark, quadrupolar mode is investigated, which produces the plasmonic analogue of electromagnetically induced transparency through the interference of the bright and dark modes. Additionally, the plasmonic resonance of a metallic nanostructure is extremely sensitive to its local dielectric environment. Vanadium dioxide exhibits a large change in its dielectric function during its metal to insulator phase transition. The combination of the gold dolmen nanostructure with vanadium dioxide produces a tunable Fano resonance. The dimensions of the structure are optimized such that the resonance is near symmetric in shape and located in the near infrared to allow for spectroscopic measurement. The author is unable to obtain experimental results of this hybrid structure, but previous work, combined with simulation data, suggest the proposed structure will exhibit the expected result.

1. INTRODUCTION

1.1 Motivation

As the field of nanotechnology grows and its applications multiply, so does the need for structures exhibiting actively modulated responses.[1] Plasmonics is one such field of interest, because plasmonic nanostructures exhibit resonances that can be tuned through changes in the geometry and the local dielectric environment of the structures. However, purely plasmonic samples have resonances which cannot be altered after fabrication. To produce reconfigurable devices, it is necessary to combine plasmonic nanostructures with an actively tunable element. For active tunability, the reversible metal-to-insulator phase transition (MIT) of vanadium dioxide (VO_2) is desirable due to its large change in dielectric function. The idea of a hybrid metal:VO_2 nanostructure combines the sensitivity of a plasmonic resonance with a tunable dielectric environment produced by the metal to insulator transition of VO_2.[2] One such hybrid geometry is that of the gold (Au):VO_2 dolmen nanostructure, which exhibits a switchable Fano resonance and is the focus of this research.

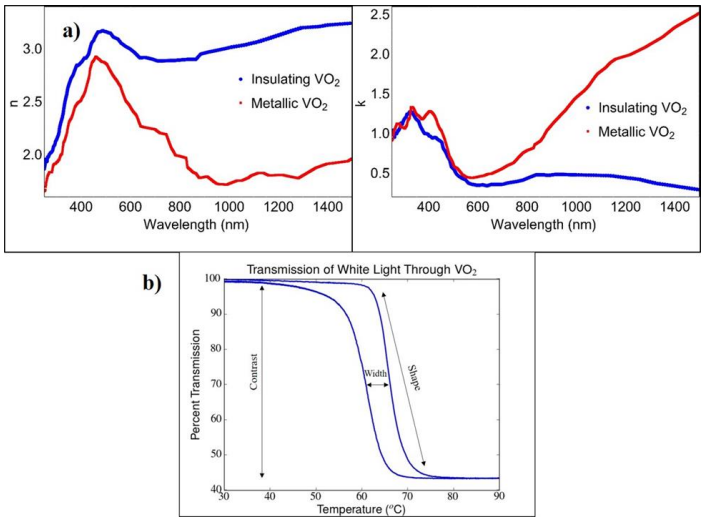

Figure 1. VO_2 properties. (a) Dielectric function of VO_2 in the insulating and metallic states. Data have been extracted from Ref. 7. (b) Characteristic hysteresis loop contrast, width and shape of an 110nm VO_2 film deposited on indium tin oxide (ITO)-covered glass by pulsed laser. Contrast, width, and shape are heavily dependent upon deposition method and annealing conditions.

The discovery of the MIT of VO_2 by Morin in 1959[3] sparked a significant amount of interest from the scientific community that continues today. The reversible MIT of VO_2 is known to occur optically on the femtosecond timescale,[4] thermally (T_c = 68ºC in bulk films),[3,5] or with an applied electric field.[6] The transition alters both the crystal and electronic structure of the VO_2, switching from an insulating monoclinic to a metallic rutile form. These changes in the dielectric function of VO_2 are most significant at near infrared wavelengths, with less variation occurring in the visible range of the spectrum (Fig. 1a).[7] The changes in the dielectric function can be observed as a hysteretic change in the transmission of light through VO_2 during the MIT. The transmission as a function of the temperature curve has a characteristic hysteresis width, shape, and contrast, which are dependent upon the thickness, deposition parameters and method, and annealing conditions (Fig 1b).[8-10]

Metallic nanoparticles excited by an incident electromagnetic field exhibit a collective oscillation of the free-electron gas in the metal known as a plasmon. This system can be imagined as a damped-driven harmonic oscillator with the driving force taking the form of the incident light's oscillating electric field, while the damping arises from interparticle forces. In metal nanostructures with dimensions of equivalent size or smaller than the wavelength of the incident light, the localized surface modes of the plasmons can exhibit resonant behavior known as a local surface plasmon resonance (LSPR), which is analogous to a resonance in a damped-driven harmonic oscillator. When optically excited at the resonant frequency, an LSPR results in a strong and locally confined electromagnetic field in the vicinity of the nanoparticle. Thus, light is intensely absorbed and scattered by nanoparticles. Generally, a LSPR exists in the visible or near infrared (NIR),[11] but LSPRs can occur in the UV[12] or the THz regime and beyond[13]. The LSPR of a metal nanoparticle is extremely sensitive to its local dielectric environment[14,15] and

the geometry[15-17] of the nanoparticle, and for this reason, can be configured as a highly tunable optical device such as a sensor. For an ideal sensor, this resonance needs to have the smallest possible full width at half maximum possible, which is produced by a resonance with low damping.

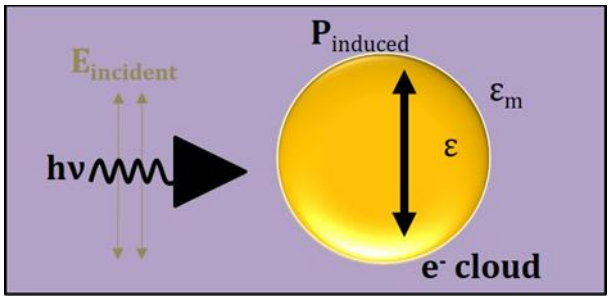

Figure 2. Schematic of oscillating electron plasma that forms a LSPR

Single nanoparticles such as disks or rods generally have broad dipolar resonances. However, when these simple nanostructures are combined into more complex multi-element geometries, which promote strong coupling among the individual elements, electromagnetic resonances can interact to mimic phenomena seen in atomic systems, e.g. electromagnetically-induced transparency (EIT) and Fano resonances.[18-20] The groupings of metal nanoparticles produces a nanoscale analog of a Fano resonance – known as plasmon-induced transparency (PIT) – which is a narrow spectral region of transparency in a broad absorption peak. This Fano resonance is due to the hybridization of the metal LSPRs of the nanoparticles in the strong coupling regime.[21] The dolmen structure, which consists of two parallel nanorods perpendicular to a third nanorod, has been a subject of interest due to its exhibition of polarization-dependent PIT.[20,22]

Whereas an EIT-exhibiting system is fixed by the properties of the atoms, the PIT of a multi-element nanoparticle has the possibility of active modulation. One significant disadvantage of purely plasmonic nanostructures is that, once fabricated, their local surface plasmon resonance

shape and position are fixed by geometry. Therefore, devices created with only metal nanoparticles must be passive. One method of turning a plasmonic structure into an active device is to incorporate a phase-change material, such as VO_2, with a tunable dielectric function. By heating the VO_2 through its MIT, it is possible to alter the dielectric environment of the metal nanoparticle. This, in turn, affects the shape and position in wavelength of the nanoparticle's LSPR, giving it a temperature-dependent tunability (Fig. 3a).

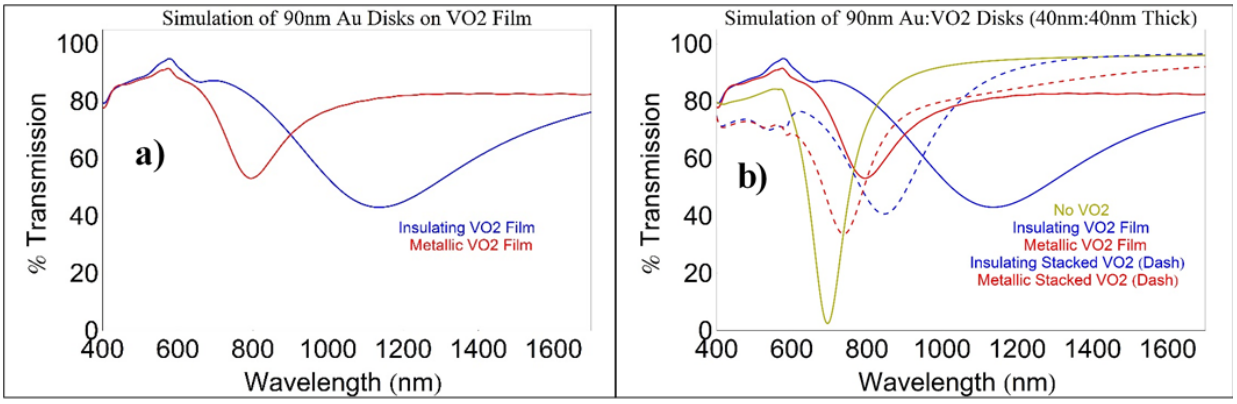

Fig. 3. a) Simulation of 40nm thick Au disks 90nm in radius on a 40nm thick VO_2 film in the insulating and metallic phases. The LSPR of the Au nanoparticle when the VO_2 is in the metallic phase is narrower and blue-shifted compared with the insulating VO_2. b) Dampening and wavelength shifting of Au:VO_2 structures compared with simple a Au disk nanoparticle. The stacked geometries broaden and damp the resonance observed in the bare Au disk less than the Au nanoparticles on a VO_2 film.

Since the VO_2 has a non-trivial imaginary part of the dielectric function, the material is lossy and causes the plasmonic resonance to broaden. This damping of the resonance can be reduced by including just enough VO_2 to produce a measurable response without broadening the resonance significantly, which can be accomplished via a stacked Au:VO_2 structure (Fig. 3b). Combining the PIT of the Au dolmen nanostructure with the dynamic functionality of VO_2 in a stacked nanoparticle geometry gives a sharp active resonance with a large change in transmission at resonance over the MIT.

1.2 PIT Mechanism

The basic optical physics of the hybrid Au:VO_2 dolmen nanostructure can be understood from the basic electromagnetic theory laid out in Ref. 20. The dolmen structure consists of a single plasmonic rod placed perpendicular and in close proximity to a double rod structure. The PIT of the dolmen structure is governed by the broad dipolar bright mode of the single rod, $|a\rangle = \tilde{a}(\omega)e^{i\omega t}$ with significant radiative loses which couples strongly with the incident electric field, $E_0 = \tilde{E}_0 e^{i\omega t}$, and a narrow quadrupolar dark mode of the double rod structure, $|b\rangle = \tilde{b}(\omega)e^{i\omega t}$, which weakly couples to the incident light and is damped by intrinsic metallic loses. If both modes are placed near to each other and are tuned to have resonant frequency, ω_0, the single rod excites the dark mode of the double rod through the near field coupling of resonating bright mode.[23] If the frequency of the incoming light, ω, is close to the resonant frequency such that the detuning is $\delta \equiv |\omega - \omega_0| \ll \omega_0$, and the damping of the two modes is such that $\gamma_b \ll \gamma_a \ll \omega_0$, then the electric field amplitudes of the two modes can be described by the linearly coupled Lorentzian oscillators of the form[21]

Equation 1

$$\begin{pmatrix} \tilde{a} \\ \tilde{b} \end{pmatrix} = -\begin{pmatrix} \delta + i\gamma_a & \kappa \\ \kappa & \delta + i\gamma_b \end{pmatrix}^{-1} \begin{pmatrix} g\tilde{E}_0 \\ 0 \end{pmatrix} \quad (2)$$

where $\tilde{a}$ and $\tilde{b}$ are the frequency-dependent field amplitudes of the bright (dipole) and dark (quadrupole) modes, respectively, κ is the coupling strength between the dipole and quadrupole antennas, which is related to their spatial separation, and g is a geometric parameter representing the strength of the dipole mode coupling to the incident electric field. The damping constants γ_a and γ_b determine the full width half maximum of the resonances. In Eq. 1, it is assumed that the dark mode does not couple with the incident light.

The top bar of the dolmen nanostructure, when oriented such that it is parallel to the incident electric field, functions as the dipole antenna into which the electric field strongly couples. However, the incident light cannot couple with the parallel bars, which function as a quadrupole antenna. Due to the small dipole-quadrupole spacing, the dipole resonance mode allows the light to couple into the dark mode, exciting a quadrupolar resonance that couples into the bright mode. The net electric field amplitude of the dolmen is given by,

Equation 2

$$\tilde{a}(\omega) = \frac{-gE_0(\delta + i\gamma_b)}{(\delta + i\gamma_a)(\delta + i\gamma_b) - \kappa^2}. \quad (2)$$

The coupling strength between the bright and dark modes governs the width and change in absorption in the PIT region, and sharpness of the resonance is governed by the losses of the dark mode which are due to the intrinsic properties of the material.

When the dolmen is fabricated on top of a VO_2 film or as a stacked Au:VO_2 structure, the plasmon resonance for both the dipole and quadrupole modes, and thus the PIT, is altered by the change in the local dielectric environment during the MIT. The resonant frequency is shifted by differences in the real part of the dielectric. Since the imaginary part of the dielectric function for VO_2 is nonzero, this also changes the relaxation rates γ_a and γ_b. Recent measurements show a roughly 30% increase in the dephasing rate for gold nanodisks with a VO_2 film, indicating a broadening of the plasmon resonance.[24] Since this is measured with only a disk, which is solely a bright mode, the VO_2 may alter the dark mode of the dolmen differently.

When the nanostructure dimensions and wavelength of incident light are appropriately tuned, the coupling of the bright mode with the incident light and the dark mode produces destructive interference in the bright mode where the amplitude of the mode goes to zero and no

longer absorbs light at that wavelength. This causes the dipole antenna to become transparent to the incident light in a narrow wavelength region (Fig 4a) and is in agreement with previous studies of dolmen-like structures.[21,25,26] The behavior can also be pictured in the plasmon mode-hybridization framework as a hybrid state of a bright dipole antenna and a dark quadrupole antenna.[23,27] A lower energy bonding state and a higher energy antibonding state, which are linear superpositions of the bright and dark mode, form. A hybrid state, associated with PIT, occurs between these states in energy, as the opposing contributions from the incident light-dipole and dipole-quadrupole mode coupling cancel each other (Fig 4b). The subradiant bonding resonance is at a lower energy, because the local charges near the dipole-quadrupole spacing have opposite signs. The super-radiant antibonding resonance is at a higher energy, because the local charges near the spacing are of like signs.

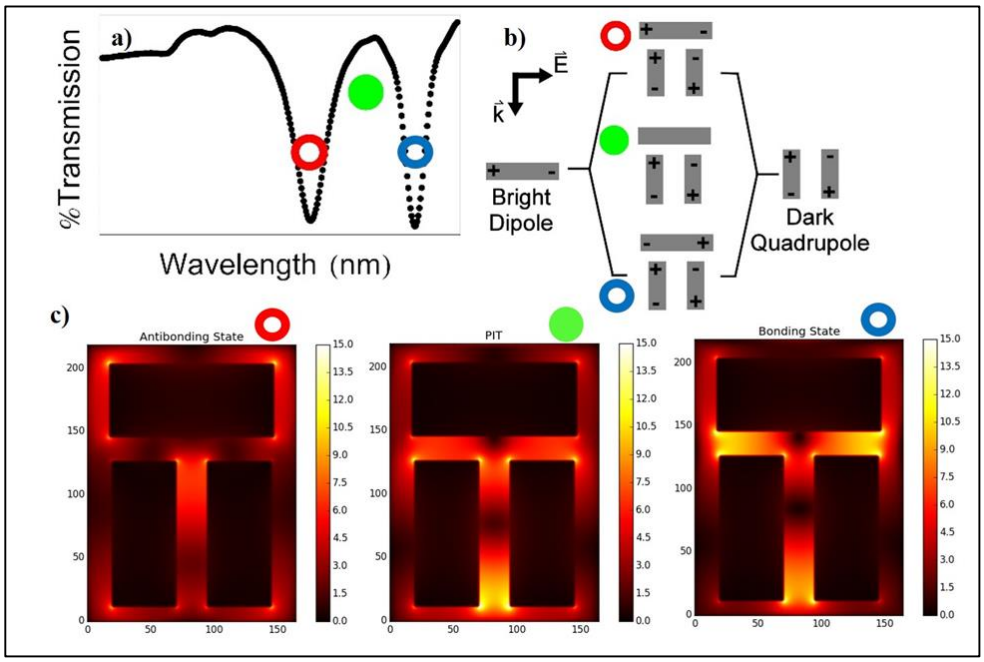

Fig 4. Dolmen structure exhibiting plasmonic analogue of EIT. a) Theoretical shape of PIT transmission spectrum. b) Plasmon mode hybridization diagram for the dolmen structure. The bright dipole mode excited by the incident light couples with the dark quadrupole mode, and this coupling forms the bonding (blue open circle) and antibonding (red open circle) states at lower and higher energies, respectively. c) Simulated 2D electric near field map from structure comprised of gold with a 38 nm gap. Light is incident to normal to the structure, and is polarized parallel to the dipole. Adapted from Ref 24.

Two-dimensional simulations of the electric near field maps of the structure (Fig 4c) demonstrate the differing behavior of the dolmen in the bonding (blue open circle), antibonding (red open circle), and PIT (green circle) states. The bonding state shows a strong electric field in the gap between the dipole and quadrupole antennas, that demonstrates the potential difference between the local charges in dipole and the quadrupole as seen in the hybridization model. The antibonding state has a strong electric field around the dipole antenna, which is being distorted in the gap by the nearby like charges of the quadrupole generating a repulsive force. These strong electric fields contribute to the absorption of the incident light by the dolmen. The PIT region exhibits very little electric field in the dipole mode, but a large electric field in the quadrupole mode. This indicates only a small portion of the light is being absorbed and subsequently emitted by the dipole in this hybridized mode.

2. METHODOLOGY

2.1 Fabrication

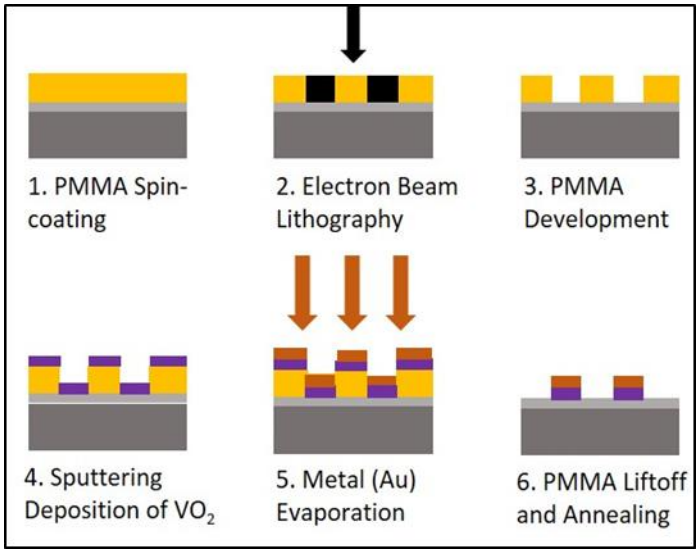

Figure 5. Fabrication of composite nanoparticles, consisting of (1, 2) EBL on spin coated PMMA, (3) PMMA development, (4) Sputtering VO_2 deposition, (5) gold evaporation, and (6) liftoff of the PMMA and residual gold/VO_2, then annealing.

Samples are fabricated on 0.5 mm thick silica glass substrates with 15-30 nm ITO coating (Delta Technologies) using a procedure similar to Fig. 5, as follows: (1) Polymethyl methacrylate (PMMA: 950 A4 at thickness of ~240nm) spin-coated on the sample, followed by (2) electron beam lithography (EBL) of 100 μm × 100 μm square arrays of nanoparticles, and by (3) chemical development using methyl isobutyl ketone:isopropyl alcohol to remove the exposed areas of PMMA. (4) Sputtering of 20nm of vanadium metal target yielding amorphous VO_2 (Sputtering conditions: 20 sccm O_2, 1 sccm Ar, deposition pressure of 6 mTorr, ~1 Å/s deposition rate of VO_2 adjusted by a proportional-integral-derivative controller and measured by a quartz crystal microbalance). (5) Thermal evaporation of 60nm of gold (1 Å/s) on the sample is followed by (6) chemical liftoff of the remaining PMMA using Remover PG™ (MicroChem Corp.), and finally thermal annealing (450°C, O_2 gas at 250 mTorr, 10min) to obtain stoichiometric, crystalline VO_2 underneath a layer of gold. The final structure is similar to that seen in Fig 6.

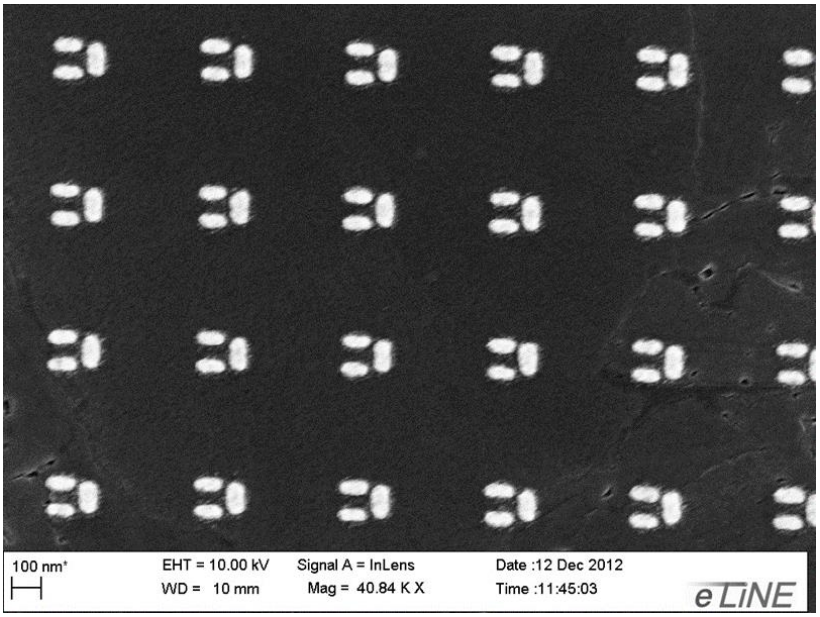

Figure 6. SEM image of Au dolmens on VO_2 film from previous dolmen study. Due to limitations of EBL, edges of rods are rounded, so the experimental data need to be compared with simulations using the fabricated dimensions for accuracy.

This multi-layer lithography procedure had been used previously to create actively modulated Au:VO_2 stacked disks structures. In (2), accelerating voltage, base dose, and PMMA thickness must be carefully tuned to obtain the 13 nm gap between the dolmen dipole and quadrupole, as touching nanoparticle components do not exhibit PIT, while still fabricating arrays with enough structures to produce a measurable signal and large enough for optical characterization.

2.2 Measurement

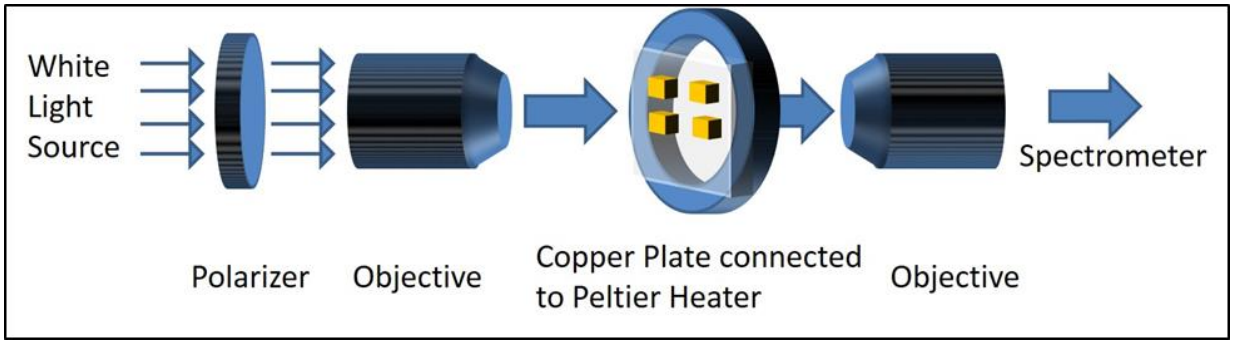

Figure 7. Schematic of transmission spectroscopy set-up. White light source passes through a polarizer, is focused to a 100 µm diameter spot size then sent through an optical cable to a spectrometer. The sample is mounted on a Peltier-heated copper plate with a hole in the center to allow for light to transmit through.

Single 100 µm nanoparticle arrays from the sample are imaged using white light spectroscopy. A white light source is polarized parallel to the axis of the dipole and focused by a 10x microscope objective, to a 100 µm diameter spot on the sample. The sample is mounted on a large copper plate connected to a Peltier heater to heat said sample. The heater and copper plate have coaxial holes through their centers to permit optical transmission measurement. Light is collected with a 5x microscope objective and transmitted via optical fiber to a Princeton Instruments Acton SpectraPro InGaAs Spectrometer with an indium gallium arsenide (InGaAs) detector that has a usable range of 800-1700 nm. To locate the arrays and ensure that the white light is focused on single arrays, a camera is mounted in reflection geometry. Spectroscopic

measurements are taken before and after the VO_2 phase transmission, at nominal temperatures of 30ºC and 90ºC.

2.3 Simulation

Three-dimensional full-field finite-difference time-domain (FDTD) simulations using Lumerical FDTD Solutions® software are performed to determine the optimal dimensions to produce strong PIT in the NIR before fabrication. Lumerical's FDTD algorithm is designed to model propagating electromagnetic waves interacting with structures within the time domain. Fourier analysis is then performed to calculate the frequency-dependent response of the geometry in question. The algorithm joins the electric and magnetic components of the differential form of Maxwell's curl equations and then alternates between solving the electric and magnetic components at each half time-step.[28] The six coupled differential equations are:

Equation 3

$$\frac{\partial E_x}{\partial t} = \frac{1}{\epsilon}\left(\frac{\partial H_z}{\partial y} - \frac{\partial H_y}{\partial z} - \sigma E_x\right) \quad (3)$$

$$\frac{\partial E_y}{\partial t} = \frac{1}{\epsilon}\left(\frac{\partial H_x}{\partial z} - \frac{\partial H_z}{\partial x} - \sigma E_y\right) \quad (4)$$

$$\frac{\partial E_z}{\partial t} = \frac{1}{\epsilon}\left(\frac{\partial H_y}{\partial x} - \frac{\partial H_x}{\partial y} - \sigma E_z\right) \quad (5)$$

$$\frac{\partial H_x}{\partial t} = \frac{1}{\mu}\left(\frac{\partial E_y}{\partial z} - \frac{\partial E_z}{\partial y} - \rho_m H_x\right) \quad (6)$$

$$\frac{\partial H_y}{\partial t} = \frac{1}{\mu}\left(\frac{\partial E_z}{\partial x} - \frac{\partial E_x}{\partial z} - \rho_m H_y\right) \quad (7)$$

$$\frac{\partial H_z}{\partial t} = \frac{1}{\mu}\left(\frac{\partial E_x}{\partial y} - \frac{\partial E_y}{\partial x} - \rho_m H_z\right) \quad (8)$$

E and *H* are the electric and magnetic fields, respectively, ε and μ are the permittivity and permeability of their respective fields, and σ is the electrical conductivity in accordance with

Ohm's law. For symmetry, and to allow for magnetic losses, a term for the magnetic resistivity, ρ_m, is also included in the equations.[28]

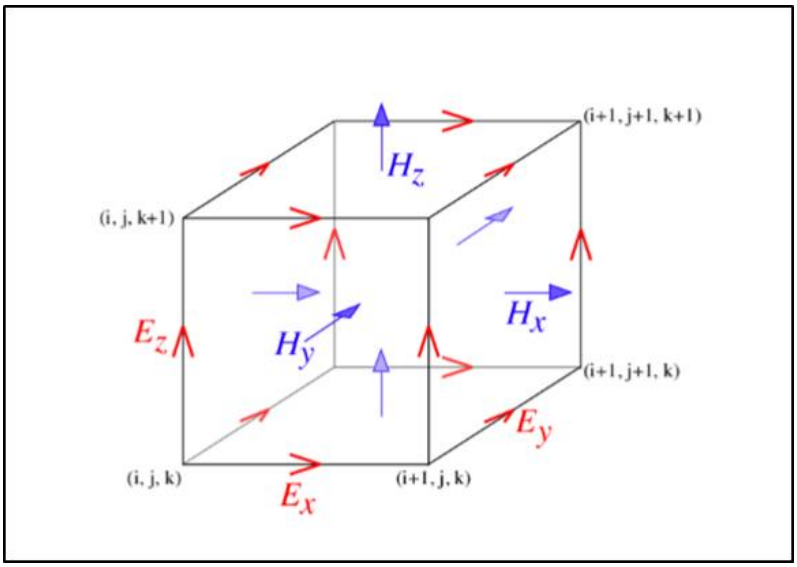

Figure 7. The Yee lattice consists of interwoven E and H field points. The E field components originate at the corners and point along the edges of the cube. The H field originate at the center of each cube face. Image used from: http://ab-initio.mit.edu/wiki/index.php/Image:Yee-cube.png.

The modeled volume needs to be discretized so that each spatial point (i, j, k) on the volume lattice corresponds to a physical point $(i\Delta x, j\Delta y, k\Delta z)$, such that a time dependent function $f(x, y, z, t)$ can be represented by $f^n = f(i\Delta x, j\Delta y, k\Delta z, n\Delta t)$. Fig 7 shows the schematic of a Yee lattice, which describes a single mesh point the FDTD volume.[28] The electric components originate from the corners of the cube, while the magnetic components originate from the cube faces. This allows the Yee algorithm to use a central difference approach with the electric and magnetic fields offset by half-steps in order to evolve the system in time. This geometry and the component equations help the model solve Faraday's and Ampere's Law so that the EM wave propagates through the object in the simulation region.

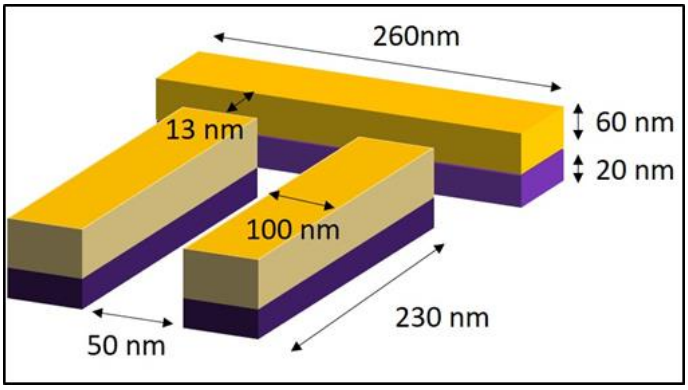

Figure 8. Simulated Au:VO_2 dolmen dimensions to produce optimal PIT in insulating and metallic phases of VO_2. Dimensions chosen from Ref. 18.

The simulation region contains the Au:VO_2 nanostructure placed on a 1500 nm thick glass substrate, and a broadband, polarized plane-wave light source incident normal to the substrate. Periodic boundary conditions are imposed to simulate an array of identical nanostructures in 400nm × 500nm unit cells. Three detectors, recording electric field as a function of wavelength and position, are located inside the nanostructure at the median z-heights of the gold, VO_2, and Au:VO_2 interface. Simulated transmission measurements are recorded with another detector placed 1300 nm below the nanostructures. An optimized transmission spectrum is considered to be where the signal reaches a maximal depth in the NIR range of our spectrometer, 800-1700nm, with symmetric decreased regions of transmission on either side of the increased PIT feature. Additionally, an override mesh surrounds the nanoparticle in order to achieve higher accuracy in immediate vicinity of the nanoparticle. The dimensions of the optimized nanostructure (dipole length and width, quadrupole length and width, spacing between the quadrupole bars, and dipole-quadrupole separation) are chosen from Verellen, *et. al.*[18] The nanostructure thickness is varied to determine the optimal Au:VO_2 thickness ratio for a strong PIT (Fig 8).

3. Results and Discussion

3.1 Simulations

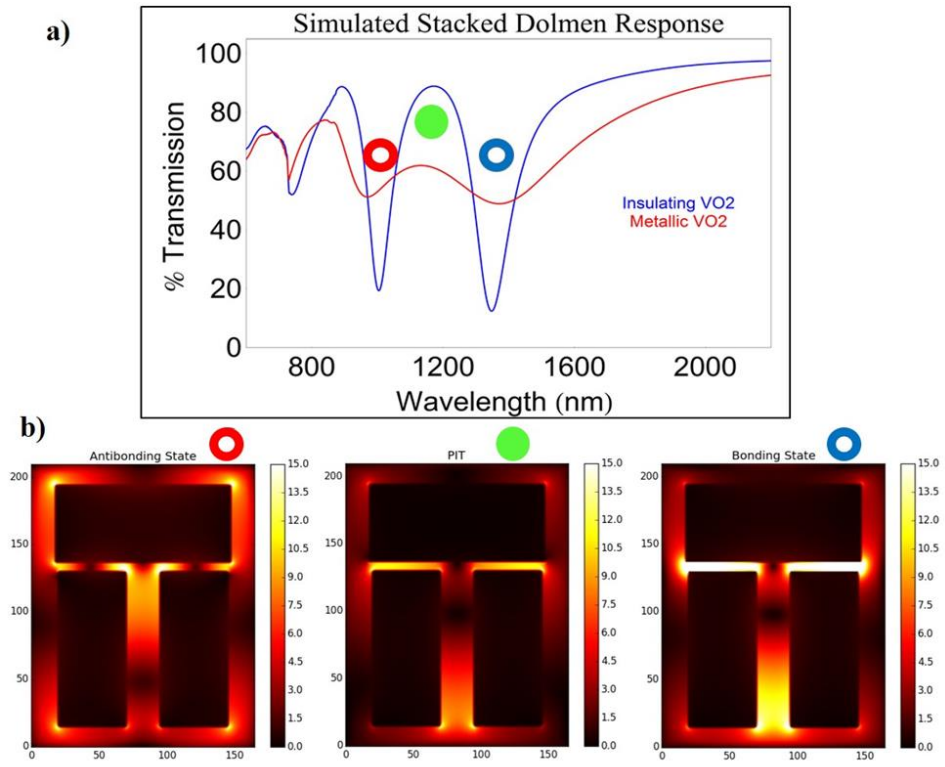

Figure 9. Simulation of optimized Au:VO_2 dolmen dimensions. a) PIT is observed in both insulating and metallic states of the VO_2. The depth of the resonance is more pronounced when the VO_2 is in the insulating phase. b) The near field maps of the simulated dolmen structures. The bonding and antibonding states have changed in energy levels from the previous studies.

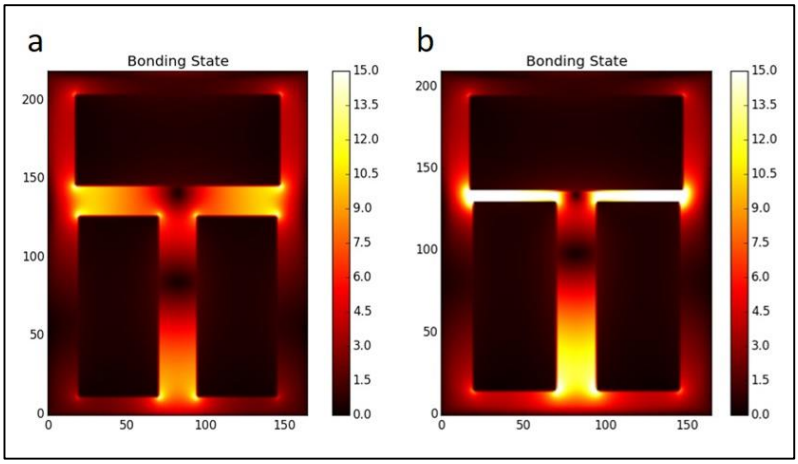

Figure 10. Comparison between dolmen structures with a) larger (38 nm) and b) smaller (13 nm) dipole-quadrupole spacing. The inner-gap intensity of the smaller gap dolmen is much higher than that that of larger gap dolmen.

The simulated dolmen structures have dimensions as shown above in Fig 8. The bonding mode of the dolmen, which corresponds to the broader resonance than that of the antibonding mode, is at a higher wavelength than the antibonding mode. The relative energy positions of the bonding and antibonding modes are in agreement with the dolmen hybridization models from previous studies.[23,26] The relative broadness of the bonding and antibonding modes are not in agreement with previous dolmen hybridization models, as the imaginary component of the dielectric function of VO_2 is not constant with wavelength, especially for metallic VO_2 in the NIR. The relative electric field intensities when compared with a dolmen structure with greater dipole-quadrupole spacing indicates that the dipole-quadrupole spacing plays a key role in the coupling and energy of the two non-PIT hybrid modes (Fig 10).

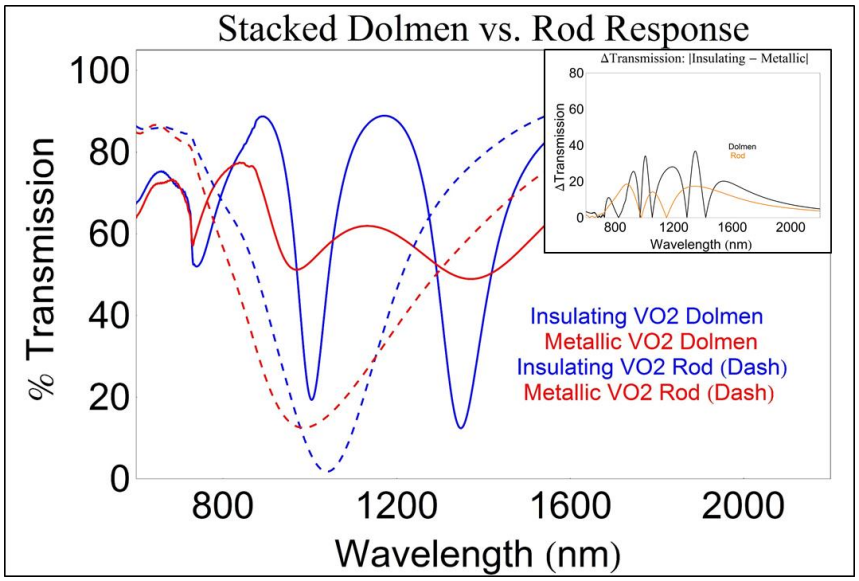

Figure 11. Comparison of the plasmonic response of Au:VO_2 dolmen and rod stacked structures. The resonant wavelength shift is comparable between the two structures. Inset: The change in transmission during the MIT of the VO_2 is greater in the dolmen structure than the VO_2 in the NIR region.

The insulating phase of the VO_2 gives the dolmen structure much sharper resonances with significantly less damping than the metallic phase of the VO_2 due to the lower imaginary part of the dielectric function of the insulating VO_2 in the NIR. Additionally, the shift in the

resonance location is on the order of tens of nanometers, which is resolvable in the experimental setup described above. The insulating phase also allows transmission of light within the PIT region to recover to nearly off-resonance transmission, while the PIT region does not retain this dramatically improved transmission when the VO_2 is in the metallic phase, which is the desired effect. When compared with the change in contrast of a single element nanostructure, for example, a dipolar Au:VO_2 stacked rod (Fig 11), it is easy to see that this complex, multi-element nanostructure exhibits a larger change in transmission (Fig 11 inset) while maintaining a similar shift in the resonance location. This change in contrast of the PIT region over the MIT of the VO_2 in the NIR can be exploited for optical sensors.

3.2 Stacked Disks

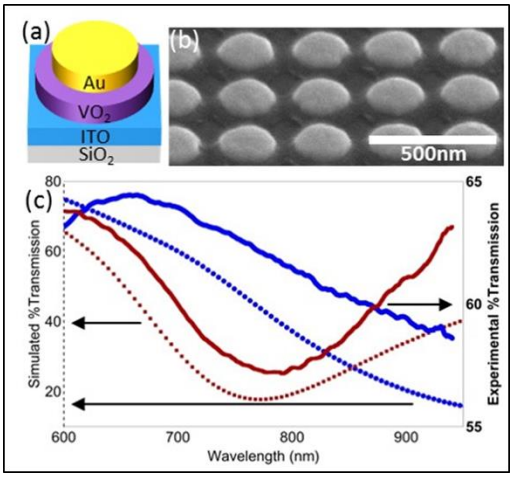

Figure 12. a) Schematic of the Au:VO_2 stacked disks on ITO-covered SiO_2. b) SEM image of Au:VO_2 stacked disks. The gold appears to rest on VO_2 disks that connect with each other at four points. c) Experimental and simulation comparison of 150nm Au:VO_2 stacked disks. The difference in simulated vs. experimental resonant wavelength is 38 nm.

Due to unforeseen delays in the EBL step, the dolmen nanostructures are unable to be fabricated. However, the fabrication process described above is nearly identical to previous stacked disk work done in the spring of 2015, which shows that the fabrication process of creating stacked Au:VO_2 nanoparticles in a single step of EBL is a viable method to produce the

stacked dolmen nanoparticles capable of producing PIT. The experimental measurements of the stacked disks are taken using the same experimental setup described in Fig 5, but an Avantes AvaSpec Spectrometer, with an effective wavelength range of 400-1000 nm, replaces the Princeton Instruments spectrometer. This limitation results in not being able to determine the agreement between the simulation and experimental results of the stacked disks when the VO_2 is in the insulating phase, but it is possible to compare the metallic state.

The fabricated Au:VO_2 disks (Fig 12a) do not have perfectly vertical side walls that are desirable for simulation accuracy. While the Au top layer remains as individual nanoparticles as expected, the widening of the VO_2 base layer causes each VO_2 disk to connect with the nearest neighbors as seen in the SEM image in Fig 12b. Therefore, the array of nanoparticles becomes more of a VO_2 film with periodic holes in between each Au disk, and not an array of Au:VO_2 stacked disk nanostructures.

The dipolar resonance of the Au:VO_2 disks appears to follow the same shape as the simulated response (Fig 12c). However, the depth of the resonance is not as pronounced when compared with simulation. The difference between the simulation and experimental result could be explained by the rounded nature of the fabricated structures, while the simulated stacked disks are still kept cylindrical in shape, or by the larger connectivity of the VO_2 layer. Additionally, the resonance shift of the Au disks from the VO_2 MIT can easily be seen in the measurement. This change in resonance position shows that the VO_2 and Au are not intermixing, and proves that this fabrication method allows for stacked structures to be fabricated via single layer EBL.

The objective of fabricating the stacked disks is to determine whether or not single layer lithography is a viable option to use for stacked structures. Previously, in order to create stacked structures with VO_2, two-layer lithography is used with the annealing of the VO_2 nanoparticles in

order to ensure that the annealing process does not cause mixing between the gold and VO_2 components of the hybrid structure. This result shows that it is possible to achieve VO_2 that maintains its phase-change properties, while only using a single layer of lithography, which makes the fabrication of the dolmen structures much simpler.

4. CONCLUSIONS

Au:VO_2 hybrid dolmen nanostructures are investigated for their active Fano resonance. Finite-difference time-domain simulations are conducted to determine the optimal Au:VO_2 stacked dolmen geometry that exhibits a narrow PIT region in the wavelength range of a Princeton spectrometer which will be used to take polarized, temperature-dependent transmission spectroscopy measurements of dolmen arrays. The stacked Au:VO_2 geometry is also shown to have sharper resonances with a smaller resonant wavelength change than Au nanoparticles on a VO_2 thin film. This allows for higher sensitivity to changes in the VO_2 dielectric function than is achievable with pure dipolar plasmon resonances.

The previous study on Au:VO_2 stacked disks shows that fabricating Au:VO_2 nanostructures in a one-step lithography process is a viable option and will allow for easier fabrication of the dolmen structures in the future. Once fabricated, measurement of the Fano resonance shift of the dolmen structures over the VO_2 MIT will allow for comparison with the simulated results. Additionally, the fabrication limits of various EBL systems can place a lower limit on the spacing between the dipole and quadrupole, but at the present moment that limit is uncertain. The understanding of these limitations and their implications on the PIT response of the dolmen structure is an important facet to understand if these structures will be used as optical sensors.

ACKNOWLEDGEMENTS

The experimental portions of this work were partially supported by a grant from the Office of Science, U. S. Department of Energy (DE-FG02-01ER45916). Thank you to Christina McGahan for guidance and support throughout the research process, and Claire Marvinney for assistance in characterization of nanoarrays.

REFERENCES

1 Zheludev, N. I. & Kivshar, Y. S. "From metamaterials to metadevices." *Nat Mater* **11**, 917-924, (2012).

2 Yang, Z., Ko, C. & Ramanathan, S. "Oxide Electronics Utilizing Ultrafast Metal-Insulator Transitions." *Annual Review of Materials Research* **41**, 337-367, (2011).

3 Morin, F. J. "Oxides Which Show a Metal-to-Insulator Transition at the Neel Temperature." *Physical Review Letters* **3**, 34-36, (1959).

4 Cavalleri, A. *et al.* "Band-Selective Measurements of Electron Dynamics in VO_2 Using Femtosecond Near-Edge X-Ray Absorption." *Physical Review Letters* **95**, 067405, (2005).

5 Suh, J. Y., Lopez, R., Feldman, L. C. & Haglund, R. F. "Semiconductor to metal phase transition in the nucleation and growth of VO_2 nanoparticles and thin films." *Journal of Applied Physics* **96**, 1209-1213, (2004).

6 Kunio, O., Yusuke, S. & Yusuke, N. "X-ray Diffraction Study of Electric Field-Induced Metal–Insulator Transition of Vanadium Dioxide Film on Sapphire Substrate." *Japanese Journal of Applied Physics* **45**, 9200, (2006).

7 Verleur, H. W., Barker, A. S. & Berglund, C. N. "Optical Properties of VO_2 between 0.25 and 5 eV." *Physical Review* **172**, 788-798, (1968).

8 Joyeeta, N. & R. F. Haglund, J. "Synthesis of vanadium dioxide thin films and nanoparticles." *Journal of Physics: Condensed Matter* **20**, 264016, (2008).

9 Nag, J., Payzant, E. A., More, K. L. & Haglund, R. F. "Enhanced performance of room-temperature-grown epitaxial thin films of vanadium dioxide." *Applied Physics Letters* **98**, 251916, (2011).

10 Marvel, R. E., Harl, R. R., Craciun, V., Rogers, B. R. & Haglund Jr, R. F. "Influence of deposition process and substrate on the phase transition of vanadium dioxide thin films." *Acta Materialia* **91**, 217-226, (2015).

11 Boltasseva, A. & Atwater, H. A. "Low-loss plasmonic metamaterials." *Science*, (2011).

12 Hu, J. *et al.* "Deep-Ultraviolet–Blue-Light Surface Plasmon Resonance of Al and Alcore/Al_2O_3 shell in Spherical and Cylindrical Nanostructures." *The Journal of Physical Chemistry C* **116**, 15584-15590, (2012).

13 Luther, J. M., Jain, P. K., Ewers, T. & Alivisatos, A. P. "Localized surface plasmon resonances arising from free carriers in doped quantum dots." *Nat Mater* **10**, 361-366, (2011).

14 Miller, M. M. & Lazarides, A. A. "Sensitivity of Metal Nanoparticle Surface Plasmon Resonance to the Dielectric Environment." *The Journal of Physical Chemistry B* **109**, 21556-21565, (2005).

15 Kelly, K. L., Coronado, E., Zhao, L. L. & Schatz, G. C. "The Optical Properties of Metal Nanoparticles: The Influence of Size, Shape, and Dielectric Environment." *The Journal of Physical Chemistry B* **107**, 668-677, (2003).

16 Mock, J. J., Barbic, M., Smith, D. R., Schultz, D. A. & Schultz, S. "Shape effects in plasmon resonance of individual colloidal silver nanoparticles." *The Journal of Chemical Physics* **116**, 6755-6759, (2002).

17 Huang, C.-p., Yin, X.-g., Huang, H. & Zhu, Y.-y. "Study of plasmon resonance in a gold nanorod with an LC circuit model." *Optical Society of America* **17**, 6407-6413, (2009).

18 Verellen, N. *et al.* "Fano Resonances in Individual Coherent Plasmonic Nanocavities." *Nano Letters* **9**, 1663-1667, (2009).

19 Gu, J. *et al.* "Active control of electromagnetically induced transparency analogue in terahertz metamaterials." *Nat Commun* **3**, 1151, (2012).

20 Luk'yanchuk, B. *et al.* "The Fano resonance in plasmonic nanostructures and metamaterials." *Nat Mater* **9**, 707-715, (2010).

21 Zhang, S., Genov, D. A., Wang, Y., Liu, M. & Zhang, X. "Plasmon-Induced Transparency in Metamaterials." *Physical Review Letters* **101**, 047401, (2008).

22 Zhu, Y., Hu, X., Fu, Y., Yang, H. & Gong, Q. "Ultralow-power and ultrafast all-optical tunable plasmon-induced transparency in metamaterials at optical communication range." *Scientific reports* **3**, (2013).

23 Ye, Z. *et al.* "Mapping the near-field dynamics in plasmon-induced transparency." *Physical Review B* **86**, 155148, (2012).

24 Ferrara, D. W., Nag, J., MacQuarrie, E. R., Kaye, A. B. & Haglund, R. F. "Plasmonic Probe of the Semiconductor to Metal Phase Transition in Vanadium Dioxide." *Nano Letters* **13**, 4169-4175, (2013).

25 Liu, N. *et al.* "Plasmonic analogue of electromagnetically induced transparency at the Drude damping limit." *Nat Mater* **8**, 758-762, (2009).

26 McGahan, C., Appavoo, K., Haglund, R. F. & Shapera, E. P. "Switchable plasmon-induced transparency in gold nanoarrays on vanadium dioxide film." *Journal of Vacuum Science & Technology B* **31**, 06FE01, (2013).

27 Prodan, E., Radloff, C., Halas, N. J. & Nordlander, P. "A Hybridization Model for the Plasmon Response of Complex Nanostructures." *Science* **302**, 419-422, (2003).

28 Taflove, A. "Review of the formulation and applications of the finite-difference time-domain method for numerical modeling of electromagnetic wave interactions with arbitrary structures." *Wave Motion* **10**, 35, (1988).